HHS Public Access

Author manuscript

Mol Cancer Ther. Author manuscript; available in PMC 2023 May 26.

Published in final edited form as:

Mol Cancer Ther. 2021 November ; 20(11): 2262–2273. doi:10.1158/1535-7163.MCT-21-0470.

Simultaneously Combined Cancer Cell- and CTLA4-Targeted NIR-PIT Causes a Synergistic Treatment Effect in Syngeneic Mouse Models

Takuya Kato[1], **Ryuhei Okada**[1], **Aki Furusawa**[1], **Fuyuki Inagaki**[1], **Hiroaki Wakiyama**[1], **Hideyuki Furumoto**[1], **Shuhei Okuyama**[1], **Hiroshi Fukushima**[1], **Peter L. Choyke**[1], **Hisataka Kobayashi**[1,*]

[1]Molecular Imaging Branch, Center for Cancer Research, National Cancer Institute, NIH, Bethesda, MD, 20892, USA

Abstract

Near-infrared photoimmunotherapy (NIR-PIT) is a new cancer treatment that utilizes antibody-IRDye700DX (IR700) conjugates. The clinical use of NIR-PIT has recently been approved in Japan for patients with inoperable head and neck cancer targeting human epidermal growth factor receptor (hEGFR). Previously cytotoxic T-lymphocyte antigen 4 (CTLA4)-targeted NIR-PIT has been shown to strongly inhibit tumor progression and prolonged survival was seen in several different tumor models due to enhanced T cell mediated antitumor immunity. In this study, combined NIR-PIT targeting CTLA4 expressing cells and cancer cells was investigated in four tumor models including a newly established hEGFR-expressing murine oropharyngeal cancer cell (mEERL-hEGFR). While single-molecule-targeted therapy (NIR-PIT targeting hEGFR or CTLA4) did not inhibit tumor progression in poorly immunogenic mEERL-hEGFR tumor, dual (CTLA4/hEGFR)-targeted NIR-PIT significantly suppressed tumor growth and prolonged survival resulting in a 38% complete response rate. After the dual-targeted NIR-PIT, depletion of CTLA4 expressing cells, which were mainly regulatory T cells (Tregs), and an increase in the $CD8^+$/Treg ratio in the tumor bed were observed, suggesting enhanced host antitumor immunity. Furthermore, dual-targeted NIR-PIT showed antitumor immunity in distant untreated tumors of the same type. Thus, simultaneous cancer cell-targeted NIR-PIT and CTLA4-targeted NIR-PIT is a promising new cancer therapy strategy, especially in poorly immunogenic tumors where NIR-PIT monotherapy is suboptimal.

Keywords

cancer; near-infrared photoimmunotherapy (NIR-PIT); target molecule; host immunity; cancer therapy

[*]**Corresponding author:** Hisataka Kobayashi, M.D., Ph.D., Molecular Imaging Branch, Center for Cancer Research, National Cancer Institute, NIH, 10 Center Drive, Bethesda, MD, 20892, USA, Tel: 240-858-3069; Fax: 240-541-4527, kobayash@mail.nih.gov.

Disclosure of Potential Conflicts of Interest: No potential conflicts of interest were disclosed.

Introduction

Near-infrared photoimmunotherapy (NIR-PIT) is a newly developed cancer treatment which induces selective cell death on targeted cells (1). A photoabsorber, which is a water-soluble silica-phthalocyanine dye named IRDye700DX (IR700), is conjugated to a monoclonal antibody (mAb) to form a resulting antibody-photoabsorber conjugate (APC) (2). APCs are intravenously injected and allowed to accumulate within tumors by binding to a cancer cell surface molecule, at which point the APC-target complexes are activated by NIR light (1,3). After exposure to NIR light, necrotic cell death is observed within several minutes selectively in cancer cells but not in surrounding normal cells (1,4,5). Cancer cell directed NIR-PIT causes rapid cellular volume expansion, rupture of cell membranes, and extrusion of antigenic cell contents into the extracellular space, causing an immunogenic cell death (ICD) (6,7). When one tumor in a bilateral tumor model was treated by NIR-PIT, the associated activation of antitumor immunity led to tumor shrinkage on the untreated side and was associated with prolonged overall survival.

Theoretically, after exposure to the NIR light, the ligand release reaction from IR700 makes the dye extremely hydrophobic, causing the aggregation of APC. This reaction causes excess tension on the cell membrane which results in physical membrane damage then necrotic cell death. Therefore, only APC-bound cells undergo necrotic cell death. Furthermore, IR700 is a water-soluble photo dye with no phototoxic or biotoxic properties of its own (8). Unbound IR700 that dissociates from the APC is safe and is readily excreted in urine (8). Thus, adjacent normal cells are unaffected by NIR-PIT. NIR-PIT is most suited to treating superficial tumors because NIR light can penetrate approximately 2 cm from the tissue surface (9,10). In more solid tissues, NIR light is rapidly attenuated. To overcome this problem, flexible, cylindrical, fiber optic, interstitial light diffusers that are inserted into the treatment site can be utilized (11). Using interstitial light diffusers practically any tumor site is amenable to NIR-PIT whether inserted via needle, catheter or endoscope. Recently, it is reported that internalized mAb-IR700 might also have cytotoxic effects after NIR light irradiation because mAb-IR700 in lysosomes induces necrotic cell death by breaking the lysosomal compartments (12). From the results of our previous experiments targeting purely internalized H-type lectin, more than 10-fold greater accumulation of APC was necessary to induce relevant cytotoxicity to transmembrane protein targeted NIR-PIT (13). Although this might add some cytotoxic effects of NIR-PIT, it is clear that NIR-PIT mainly induces plasma membrane damage after NIR light irradiation.

Epidermal growth factor receptor (EGFR) is part of the human epidermal growth factor receptor family and can form heterodimers with human epidermal growth factor receptor 2 (HER2) and other HER family members (14,15). It is known that EGFR is overexpressed in many kinds of cancers especially in squamous cell carcinoma. Currently, a global phase III clinical trial of NIR-PIT for inoperable head and neck cancer using an anti-EGFR-antibody-IR700 is currently underway (https://clinicaltrials.gov/ct2/show/NCT03769506). In Japan, the first APC (ASP-1929, Akalux™, Rakten Medical Inc.) targeting EGFR and the NIR laser system (BioBlade™, Rakten Medical Inc.) were approved for clinical use in September 2020. NIR-PIT is capable of targeting many other cancer markers, such as CD44, prostate-

specific membrane antigen (PSMA), and carcinoembryonic antigen (CEA), and thus could be widely applicable (7,16–23).

Ipilimumab is a monoclonal antibody against cytotoxic T-lymphocyte antigen protein 4 (CTLA4) and was approved in March 2011 to treat patients with late-stage melanoma. This agent was merely the first of a large class of immune checkpoint inhibitor (ICI) that have been introduced over the last decade. While these agents have been highly effective in some patients, immunotherapy-related side effects, termed immune-related adverse events (irAEs), have been widely reported in various organs (24). irAEs occur because, in addition to activating local antitumor host immunity, ICIs also activate systemic immunity, resulting in autoimmune irAEs. An ideal immune therapy should kill only cancer cells, while maintaining a normal systemic antitumor immunity.

NIR-PIT can also selectively kill many types of cells within the tumor microenvironment (TME) by targeting specific antigens (25). Recently, we reported that CTLA4-targeted NIR-PIT can effectively treat tumors by blocking the CTLA4-axis as well as by eliminating CTLA4-expressing immune suppressor cells, the majority of which are Tregs, resulting in augmentation of T cell mediated antitumor immunity (26). Thus, CTLA4-targeted NIR-PIT is a promising direction for NIR-PIT.

NIR-PIT can simultaneously target multiple antigens if a cocktail of multiple mAb-IR700 conjugates is injected. For instance, CD25-targeted NIR-PIT has shown superior effects when it is combined with cancer cell-targeted NIR-PIT, such as CD44-targeted NIR-PIT or human EGFR (hEGFR)-targeted NIR-PIT (27,28). This kind of research requires syngeneic tumor models with intact host immunity. We have recently established a hEGFR-expressing murine oropharyngeal HPV-related cancer cell (mEERL-hEGFR) (28). This is an ideal model for evaluating the immune response after NIR-PIT as a mouse tumor model for simulating the clinical setting of hEGFR-targeted NIR-PIT, because hEGFR is not expressed on murine cells therefore hEGFR-targeted NIR-PIT does not cause off-target effects to damage host immune cells. The aim of this study is to investigate the therapeutic potential of CTLA4-targeted NIR-PIT in combination with hEGFR-targeted NIR-PIT in mEERL-hEGFR or CD44-targeted NIR-PIT in other syngeneic tumor models. In this study, we used panitumumab as anti-hEGFR antibody since it has been widely used in the clinical setting.

Materials and Methods

Reagents

Water-soluble, silicon phthalocyanine derivative, IRDye700DX NHS ester (IR700), was obtained from LI-COR Bioscience (Lincoln, NE, USA). Panitumumab, a fully humanized IgG2 mAb directed against hEGFR, was purchased from Amgen (Thousand Oaks, CA, USA). Anti-mouse/human CD44 (clone IM7, RRID: AB_1107649) and anti-mouse CTLA4 (clone 9D9, RRID: AB_10949609) were purchased from Bio X Cell (Lebanon, NH, USA). All other chemicals were of reagent grade.

Synthesis of IR700-conjugated panitumumab, anti-CD44, and anti-CTLA4

Conjugation of IR700 with mAbs was performed according to previous reports. Briefly, 1 mg of either mAb was incubated with 5-fold molar excess of IR700 (10 mmol/L in DMSO) in 0.1 mol/L Na_2HPO_4 (pH 8.5) at room temperature for 1 hour. The mixture was purified with a filtration column (Sephadex G 25 column, PD-10: GE Healthcare, Piscataway, NJ, USA). The quality of APC was evaluated with Sodium dodecyl sulfate polyacrylamide gel electrophoresis (SDS-PAGE) with a 4–20% gradient polyacrylamide gel (Life Technologies, Gaithersburg, MD, USA). Non-conjugated antibody was used for the control. After electrophoresis at 80 V for 2.5 h, the gel was observed with a Pearl Imager (LI-COR Biosciences, Lincoln, NE, USA) using the 700 nm fluorescence channel. The gel was then stained with colloidal blue to compare the molecular weight of the conjugate to that of non-conjugated antibody. We abbreviate panitumumab-IR700 as pan-IR700, anti-CD44-antibody-IR700 as CD44-IR700, and anti-CTLA4-antibody-IR700 as CTLA4-IR700, respectively.

Cell culture

Parental mEERL cells were established by transduction of HPV 16 E6/E7 and hRAS to C57BL/6-derived oropharyngeal epithelial cells (29–31). hEGFR expressing murine oropharyngeal syngeneic tumor cells (mEERL-hEGFR) were a kind gift from Dr. William C. Spanos (Sanford Research, SD, USA) (28). Additionally, MC38 cells (colon cancer, RRID: CVCL_B288; kind gift from Claudia Palena, NCI, 2015) and MOC2 cells [oral cancer. RRID: CVCL_ZD33; purchased from Kerafast (Boston, MA, USA)] stably expressing luciferase (MC38-luc and MOC2-luc, generated via stable transduction with RediFect Red-Fluc lentivirus from PerkinElmer per manufacturer recommendations), and LL/2-luc cells [Lewis lung carcinoma, RRID: CVCL_A4CM; purchased from Imanis Life Sciences (Rochester, MN, USA)] were used in this study. High luciferase expression on the MC38-luc, MOC2-luc, and LL/2-luc cells were confirmed through 10 passages. mEERL-hEGFR cells were cultured in RPMI 1640 (Thermo Fisher Scientific) supplemented with 10% FBS, 1% penicillin–streptomycin (Thermo Fisher Scientific), and 1× human keratinocyte growth supplement (Thermo Fisher Scientific), which was modified from a previous report (32). MC38-luc and LL/2-luc cells were cultured in RPMI 1640 supplemented with 10% FBS and 1% penicillin–streptomycin. MOC2-luc cells were cultured in the mixture of IMDM medium and Ham's Nutrient Mixture F12 Media (at a ratio of 2:1, GE Health Healthcare Life Sciences) supplemented with 5% fetal bovine serum, 1% penicillin/streptomycin, 5 ng/mL insulin (MilliporeSigma, Burlington, MA, USA), 40 ng/mL hydrocortisone (MilliporeSigma), and 3.5 ng/mL human recombinant EGF (MilliporeSigma). All cells were cultured in a humidified incubator at 37 °C in an atmosphere of 95% air and 5% CO_2 cultured for no more than 30 passages. Cell line identity was tested via STR profiling. For MC38-luc, MOC2-luc and LL2-luc, the matching score was above 80% indicating the cell line identity was authentic (June 2021, IDEXX Bioanalytics). For mEERL-hEGFR, STR profile did not match any known cell lines (April 2021, ATCC). Mycoplasma testing was performed by PCR for MC38-luc, MOC2-luc and LL2-luc (June 2021, IDEXX Bioanalytics), by MycoAlert PLUS Mycoplasma Detection Kit (June 2021, Lonza) and all the cell lines were tested negative.

Animal and tumor model

All procedures were performed in compliance with the Guide for the Care and Use of Laboratory Animals and approved by the National Cancer Institute Animal Care and Use Committee (MIP-003; project number P183735). 6- to 8-week-old female C57BL/6 mice (RRID: IMSR_JAX: 000664) were purchased from The Jackson Laboratory (Bar Harbor, ME, USA). During invasive procedures, mice were anesthetized with inhaled 3% isoflurane and/or via intraperitoneal injection of 750 μg sodium pentobarbital (Nembutal Sodium Solution, Ovation Pharmaceuticals Inc., Deerfield, IL, USA). The lower part of the body of the mice was shaved before NIR light irradiation and image analysis. Tumors were established via subcutaneous injection of 1×10^6 cells in the right or both side of dorsal flank for each model. Mice with tumors reaching approximately 50–100 mm^3 in volume were used for the experiments. Mice were monitored each day and tumor volume (length × $width^2$ × 0.5) was measured twice a week until the tumor volume reached 2,000 mm^3, whereupon the mice were euthanized with inhalation of carbon dioxide gas. In bilateral model, the mice were euthanized when either tumor reached its humane endpoint. Tumor disappearance for 4 weeks or longer after treatment was defined as complete remission.

In vitro NIR-PIT

mEERL-hEGFR cells (2×10^5) were seeded into 12-well plates, incubated for 24 hours, and then exposed to media containing pan-IR700 or CD44-IR700 (10 μg/mL) for 1 hour at 37℃. After washing with PBS, phenol-red-free RPMI 1640 medium (Thermo Fisher Scientific) was added. NIR light (690 nm) was irradiated to cancer cells with an ML7710 laser system (Modulight, Tampere, Finland) at a power density of 150 mW/cm^2. One hour after NIR-PIT, the cells were collected with trypsin, and stained with propidium iodide (PI, 1 μg/mL) at room temperature for 5 minutes, and then assessed for PI positivity by BD FACSCalibur (BD Biosciences, San Jose, CA, USA) and CellQuest software (BD Biosciences) using FlowJo software (FlowJo LLC, Ashland, OR, USA). To assess cell viability, cell proliferation was evaluated by 3-(4,5-Dimethyl-2-thiazolyl)-2,5-diphenyl-2H-tetrazolium bromide (MTT) assay. Cells were incubated and treated, as described above. One hour after NIR-PIT, the medium was removed and 500 μL (0.5 mg/mL) of MTT reagent (SIGMA Aldrich, St. Louis, MO, USA) was added to each well. One hour after incubation, the supernatant was removed and 500 μL of 2-propanol was added to each well to dissolve the crystal formazan dye. After transferring 100 μL of the supernatant to 96 well plate, each absorbance was measured at 570 nm on a microplate reader (Synergy H1; BioTek, Winooski, VT, USA). For relative quantification, the value of absorbance in each group was normalized to that in the control group.

In vivo NIR-PIT

For the dual-targeted NIR-PIT experiment, tumor-bearing mice were randomized into four groups and intravenous injection of mixed antibody/APC followed by NIR light exposure was performed as follows: i) mixed 25 μg panitumumab and 25 μg anti-CTLA4-antibody (I.V. group), ii) mixed 25 μg pan-IR700 and 25 μg anti-CTLA4-antibody (Panitumumab NIR-PIT group), iii) mixed 25 μg panitumumab and 25 μg CTLA4-IR700 (CTLA4 NIR-PIT group), and iv) mixed 25 μg pan-IR700 and 25 μg CTLA4-IR700 (Dual NIR-PIT group).

For the monotherapy of CTLA4-targeted NIR-PIT experiment, tumor-bearing mice were also randomized into three groups as follows: i) no treatment (control group), ii) intravenous administration of CTLA4-IR700 (25 μg) without NIR light exposure (APC I.V. group), and iii) intravenous administration of CTLA4-IR700 (50 μg) followed by NIR light exposure (NIR-PIT group). The mixed antibody/APC was injected 6 days after inoculation of cancer cells into C57BL/6 mice. 24 hours after administration, NIR light (690 nm, 150 mW/cm^2) was irradiated to tumors at 50 J/cm^2 in all groups. The surface of the mouse other than the tumor was covered with aluminum foil. The mice cleared tumors in dual NIR-PIT group were re-inoculated with a subcutaneous injection of mEERL-hEGFR cells (1×10^6) in the contralateral flank. In the bilateral model, NIR light (690 nm, 150 mW/cm^2) was given only to right-sided tumors at 50 J/cm^2 and the remainder of the mouse (including the left-sided tumor) was covered with aluminum foil during irradiation.

Histologic analysis

Tumors from the mEERL-hEGFR model were harvested, formalin-fixed and paraffin-embedded, and thinly sectioned. Following standard hematoxylin and eosin (H-E) staining, bright-light photomicrographs were obtained using Mantra Quantitative Pathology Workstation (Akoya Biosciences, Menlo Park, CA, USA).

Multiplex immunohistochemistry

Multiplex immunohistochemistry (IHC) was performed using Opal 7-Color Automation IHC Kit (Akoya Biosciences, Hopkinton, MA, USA) and BOND RXm auto stainer (Leica Biosystems, Wetzlar, Germany). The following antibodies and DAPI were used: anti-CD8 (clone EPR20305, RRID: AB_2860566; Abcam, 1:500 dilution), anti-CD4 (clone EPR19514, RRID: AB_2686917; Abcam, 1:1,000 dilution), anti-FoxP3 (clone 1054C; Novus Biologicals, 1:1,000 dilution), anti-pan cytokeratin (pCK, rabbit poly, RRID: AB_10855057; Bioss, 1:500 dilution). The staining was performed according to the Opal 7-color protocol provided by the manufacturer with following modification: i) antigen retrieval was performed using BOND ER2 solution (Leica Biosystems) for 20 minutes and ii) the ImmPRESS HRP anti-Rabbit IgG (Peroxidase) Polymer Detection Kit (RRID: AB_2631198, Vector Laboratories, Burlingame, CA, USA) was used instead of anti-mouse/human secondary antibody provided in the kit. Stained slides were mounted with VECTASHIELD Hardset Antifade Mounting Medium (RRID: AB_2336787, Vector Laboratories) and then imaged using Mantra Quantitative Pathology Workstation (PerkinElmer). Images were analyzed with inForm software (RRID: SCR_019155, AKOYA Biosystems). inForm software was trained to automatically detect tissues and cell phenotype according to the following criteria: areas with pan-cytokeratin expression = tumor, other areas = stroma, $CD4^+FoxP3^+$ cells = Tregs, $CD4^+FoxP3^-$ = $CD4^+$ T cells, or $CD8^+$ = $CD8^+$ T cells, respectively. Cell count of each phenotype was exported and shown as count per mm^2. Five tumor samples were tested for each group. Five pictures were taken for each specimen and cell count and tissue area were combined for all five pictures.

Flow cytometric analysis

To evaluate expression of CTLA4, the mEERL-hEGFR tumor bearing-mice were euthanized when the established tumor volume reached approximately 150 mm^3. To confirm the loss

of CTLA4 expressing cells after NIR-PIT, the tumors of mEERL-hEGFR were harvested 3 hours after NIR light exposure. Tumor draining lymph nodes and spleens were also analyzed to evaluate for systemic effects. To assess the immune reaction in the regional lymph nodes, an ipsilateral inguinal lymph node, was harvested 2 day after NIR-PIT. Single-cell suspensions from tumor samples were prepared using the following protocol. Whole tumors were incubated in the RPMI 1640 medium (Thermo Fisher Scientific) containing collagenase type IV (1 mg/mL; Thermo Fisher Scientific) and DNase I (20 μg/mL; Millipore Sigma) at 37℃ for 30 minutes, then gently cut with scissors and mashed with the back of the plunger of a 3 mL syringe. The tissues were passed through a 70 μm cell strainer (Corning, Corning, NY, USA). Splenocytes were also analyzed to detect systemic effects. A total of 3.0×10^6 cells was stained and data for 5.0×10^5 cells were collected for each tumor. For lymph node and spleen, a total of 1.0×10^6 cells was stained and data for 1.0×10^5 cells were collected. The cells were stained with antibodies, purchased from either BioLegend [anti-CD3e (145–2C11, RRID: AB_312660), anti-CD8α (53–6.7, RRID: AB_2888883), anti-CD11b (M1/70, RRID: AB_312791), anti-CD11c (N418, RRID: AB_314173), anti-CD25 (PC61.5, RRID: AB_312847), anti-F4/80 (BM8, RRID: AB_893481), anti-CD45 (30-F11, RRID: AB_2563598), and anti-I-A/I-E (M5/114.15.2, RRID: AB_313328)] or from Thermo Fisher Scientific [anti-CD4 (RM4–5, RRID: AB_464902), anti-CD69 (H1.2F3, RRID: AB_1210795), and anti-NK1.1 (136, RRID: AB_2534431)]. To distinguish live from dead cells, cells were also stained with LIVE/DEAD Fixable Dead Cell Stain (Thermo Fisher Scientific). To assess CTLA4 expression, anti-CTLA4 (9D9) or an isotype control [murine IgG2b (MPC-11, RRID: AB_1107791); Bio X Cell] was conjugated with Alexa Flour 647 NHS ester (Thermo Fisher Scientific). The conjugation was performed with the same method as that used for staining FoxP3, the cells were fixed and permeabilized with FoxP3 Transcription Factor Staining Buffer Set (Thermo Fisher Scientific) followed by incubation with anti-FoxP3 (FJK-16s; Thermo Fisher Scientific). The fluorescence of the cells was then analyzed with the flow cytometer (FACSCalibur or FACSLyric, RRID: SCR_000401, BD Biosciences) and FlowJo software (FlowJo LLC, RRID: SCR_008520). Dead cells were removed from analysis based on FSC, SSC, and staining with LIVE/DEAD Fixable Dead Cell Stain. The Treg population was defined by gating for $CD4^+FoxP3^+$ T cells among $CD3^+$ T cells.

Statistical analysis

Quantitative data were expressed as means ± SEM. For *in vitro* experiments, a one-way analysis of variance (ANOVA) followed by the Tukey's test was used. For *in vivo* experiments, a two-way repeated measures ANOVA followed by the Tukey's test was used for multiple comparisons (more than 3 groups). The cumulative probability of survival was analyzed by the Kaplan–Meier survival curve analysis, and the results were compared with the log-rank test followed by Bonferroni correction. Statistical analysis was performed with GraphPad Prism version 8 (GraphPad software, RRID: SCR_002798, La Jolla, CA, USA). A P value of less than 0.05 was considered statistically significant.

Results

Efficacy of panitumumab and CTLA4-targeted NIR-PIT for mEERL-hEGFR cells *in vitro*

To confirm conjugation of IR700 dye and panitumumab or anti-CTLA4 antibody, SDS-page was used. Pan-IR700 and nonconjugated panitumumab showed nearly identical molecular weight, but pan-IR700 demonstrated strong 700 nm fluorescent intensity (Fig. 1A). CTLA4-IR700, demonstrated similar findings. Based on incorporation of PI and MTT assay, cancer cell death was induced by NIR-PIT in a NIR light-dose dependent manner in mEERL-hEGFR mice exposed to pan-IR700 (Fig. 1B and C). Neither NIR light alone nor pan-IR700 alone induced significant effect on cell viability. Additionally, no significant cell damage was detected in mEERL-hEGFR cells when performing CTLA4-targeted NIR-PIT. These data validated that hEGFR-targeted NIR-PIT induced target cell-specific cell death in mEERL-hEGFR cells, whereas CTLA4-targeted NIR-PIT did not affect mEERL-hEGFR cells *in vitro*.

Panitumumab NIR-PIT immediately destroys tumor cells *in vivo*.

Next, we evaluated cell damage in mEERL-hEGFR tumors after each NIR-PIT treatment by histological analysis. Tumors were harvested 1 hour after light exposure. H-E staining demonstrated swelling and vacuolation of the tumor cell in panitumumab NIR-PIT treated tumors, but no obvious change was found in CTLA4-targeted NIR-PIT treated tumors (Fig. 1D). Thus, pathological data demonstrated that panitumumab NIR-PIT caused the immediate death of the tumor cell but CTLA4 NIR-PIT did not.

Fewer tumor infiltrating T cells in mEERL-hEGFR tumor

To compare the immunogenicity of various tumor models, we examined $CD8^+$ tumor infiltrating T cells (TILs) in three murine syngeneic tumor models, LL/2-luc, MC38-luc, and mEERL-hEGFR tumors by IHC. The number of $CD8^+$ TILs in mEERL-hEGFR tumors was lower than that of other two tumor models (Fig. 1E). Next, we evaluated the $CD8^+$/$CD4^+FoxP3^+$ (Treg) ratio of TILs, because this ratio is known to be an indicator of a robust antitumor immune response (33.). The intratumoral $CD8^+$/Treg ratio was also significantly lower in mEERL-hEGFR tumor than in the other two tumors. These results suggested that mEERL-hEGFR tumor was poorly immunogenic compared to other syngeneic tumor models.

Tregs express CTLA4 within the tumor bed

To find out which type of cells expressed CTLA4 *in vivo*, CTLA4 expression of various cell types from mEERL-hEGFR tumors was analyzed by flow cytometry. CTLA4 expression was negligible or minimal on mEERL-hEGFR cells ($hEGFR^+CD45^-$), myeloid cells ($CD3^-CD11b^+$), cytotoxic T cells ($CD3^+CD8^+$), and helper T cells ($CD3^+CD4^+FoxP3^-$) (Fig. 2A). In Tregs ($CD3^+CD4^+FoxP3^+$), CTLA4 was highly expressed, and the relative fluorescence intensity (RFI) of Tregs was significantly higher than that of other cell types.

Depletion of Treg cells within tumor after CTLA4 targeted NIR-PIT

Next, selective depletion of CTLA4 expressing cells was evaluated in tumors, tumor draining lymph nodes, and spleens after each NIR-PIT by flow cytometry (Fig. 2B). The treatment efficacy was compared among four groups; panitumumab and anti-CTLA4 antibody injection (I.V. group), pan-IR700 and anti-CTLA4 antibody injection (pan NIR-PIT group), panitumumab and CTLA4-IR700 injection (CTLA4 NIR-PIT group), and the combination of pan-IR700 and CTLA4-IR700 injection (dual NIR-PIT group). NIR light was applied to all groups one day after injection. CTLA4 expressing cells within the tumor were decreased in the CTLA4 NIR-PIT and dual NIR-PIT groups compared to I.V. group, but no significant changes were detected in regional lymph node or spleen (Fig. 2C). Next, we assessed which type of T cells were selectively depleted by NIR-PIT. Tregs were significantly reduced in the CTLA4 NIR-PIT and dual NIR-PIT groups (Fig. 2D and E). The populations of $CD4^+FoxP3^-$ and $CD8^+$ T cells remained intact. For this result, the ratios of $CD4^+FoxP3^-$/Tregs and $CD8^+$/Tregs were increased (Fig. 2E). In lymph node and spleen, no significant changes were observed in each monotherapy of NIR-PIT groups compared to I.V. group. These results showed that CTLA4-targeted NIR-PIT, both as monotherapy and as combination with panitumumab NIR-PIT, mainly depleted Tregs and this effect was limited to the treatment site.

In vivo 700 nm fluorescence imaging studies of mEERL-hEGFR cells

To evaluate the accumulation of each APC within the tumor, serial fluorescence images of 700 nm were obtained. The fluorescence intensity of both pan-IR700 and CTLA4-IR700 in mEERL-hEGFR tumors showed peak intensities within 1 day after APC injection, which decreased gradually over the following days (Supplementary Fig. S1). TBR showed a similar trend. Thus, NIR light exposure was given one day after APC injection so as to achieve the maximal contrast between tumor and background normal tissue.

The efficacy of CTLA4-targeted NIR-PIT in mEERL-hEGFR tumors

We evaluated the antitumor effect of the monotherapy of CTLA4-targeted NIR-PIT for mEERL-hEGFR tumor. The treatment and imaging regimen are shown in Fig. 3A. The treatment efficacy was compared among three groups; non-treatment group (control group), APC injection without NIR light irradiation (APC I.V. group), and APC injection followed by NIR light irradiation (NIR-PIT group). One day after injection of CTLA4-IR700, the tumors in APC I.V. and NIR-PIT groups showed high 700 nm fluorescence intensity, whereas no 700 nm fluorescence was detected in the control group (Fig. 3B). After NIR light exposure to 50 J/cm^2, 700 nm fluorescence signal of the tumor in NIR-PIT group decreased immediately, while it was not changed in APC I.V. group (Fig. 3B). Tumor growth was slightly inhibited in the APC I.V. or NIR-PIT groups compared with the control group, but no significant difference was detected (Fig. 3C). In the survival curve, the NIR-PIT group did not show improved survival compared to other groups (Fig. 3D). These results demonstrated that there was no significant therapeutic effect of CTLA4-targered NIT-PIT alone in the mEERL-hEGFR allograft model.

Simultaneous dual NIR-PIT targeting hEGFR and CTLA4 inhibits tumor growth better than either single-molecule-targeted therapy alone

To evaluate the efficacy of simultaneous CTLA4/hEGFR dual-targeted NIR-PIT against mEERL-hEGFR tumor, we performed *in vivo* experiments among four groups as described above. The treatment and imaging regimen are shown in Fig. 4A. 700 nm fluorescence at the tumor site was detected in the groups injected with APCs (panitumumab NIR-PIT, CTLA4 NIR-PIT, and dual NIR-PIT groups), and this signal immediately decreased after NIR light exposure (Fig. 4B). The tumor volume in the dual NIR-PIT group was also significantly decreased as compared to any other groups ($p < 0.001$, each group vs. the dual NIR-PIT group) (Fig. 4C). Tumor progression in both panitumumab and CTLA4 NIR-PIT groups was not significantly decreased compared with the I.V. group. Furthermore, the dual NIR-PIT group achieved significantly prolonged survival compared with the I.V. group ($p < 0.01$) and the panitumumab NIR-PIT group ($p < 0.05$) (Fig. 4D). Although the survival of the dual NIR-PIT group was not significantly prolonged as compared to the CTLA4 NIR-PIT group, a larger number of the tumors was cleared in the dual NIR-PIT group than in the CTLA4 NIR-PIT group (38% vs. 25%). In order to evaluate the combined effect of CTLA4-targeted NIR-PIT and other cancer cell-targeted NIR-PIT, we investigated the efficacy of dual NIR-PIT utilizing CD44 and CTLA4 antibodies in LL/2-luc, MC38-luc, and MOC2-luc tumors (Supplementary Fig. S2). CTLA4/CD44 dual NIR-PIT group significantly inhibited tumor progression compared to the I.V. group in all tumor models and prolonged the survival in LL/2-luc and MC38-luc tumors. CTLA4/CD44 dual-targeted NIR-PIT eradicated 44% and 40% of established LL/2-luc and MC38-luc tumors respectively, however, no additional effect was observed between CTLA4-targeted NIR-PIT monotherapy and CTLA4/CD44 dual-targeted NIR-PIT in all tumor models.

Dual-targeted NIR-PIT activates antitumor host immunity

To assess the activation of dendritic cells (DCs) and $CD8^+$ T cells after each NIR-PIT, the ipsilateral inguinal lymph nodes were harvested 2 days after NIR-PIT, and analyzed by flow cytometry. The mean fluorescence intensity (MFI) of CD40 and CD80 in DCs was significantly higher in the dual NIR-PIT group compared with no treatment group (control group) (Fig. 5A and B). In CD86, the MFI in the dual group was higher than that of any other group (Fig. 5C). Furthermore, the percentage of $CD25^+$ cells among $CD8^+$ T cells within lymph nodes was significantly higher in all groups treated by NIR-PIT compared with the I.V. group (Supplementary Fig. S3). These results suggested that DC maturation and activation of cytotoxic T cell response against the cancer cells was enhanced by activated DCs after dual-targeted NIR-PIT.

Dual-targeted NIR-PIT leads to accumulation of $CD8^+$ T cells in tumor tissue

To evaluate the accumulation of lymphocytes in the TME after each therapy, we analyzed TILs by multiplex IHC (Fig. 5D and E). $CD8^+$, $CD4^+FoxP3^-$, and $CD4^+FoxP3^+$ T cells were counted for each specimen. $CD8^+$ T cells had a significantly higher density in the dual NIR-PIT group compared to the control group (Fig. 5F), whereas $CD8^+$/Treg ratio in the dual NIR-PIT group was significantly higher than all other groups (Fig. 5G). These results demonstrated that dual-targeted NIR-PIT reversed the immunosuppressive TME,

resulting in T cell activation which strongly suppressed tumor progression compared to either single-molecule-targeted therapy.

Dual-targeted NIR-PIT results in immunologic memory

To examine the presence of immunological memory, mice whose treated mEERL-hEGFR tumors disappeared after dual NIR-PIT were re-inoculated with mEERL-hEGFR cells approximately 15 weeks after the initial NIR-PIT on the contralateral dorsum (Fig. 6A). All mice that had cleared the previously inoculated tumor by dual-targeted NIR-PIT rejected the newly implanted mEERL-hEGFR cells completely, whereas no rejection was observed in untreated control mice (Fig. 6B and C). These results suggest the development of immunologic memory after dual-targeted NIR-PIT.

Dual-targeted NIR-PIT demonstrates abscopal effect in a bilateral tumor model

To assess the development of systemic antitumor immunity, a bilateral mEERL-hEGFR tumor model was established, and the treatment efficacy was compared between I.V. group and dual NIR-PIT group. The treatment and imaging regimen are shown in Supplementary Fig. S4A. The contralateral tumors were shielded from NIR light exposure (Supplementary Fig. S4B). After exposure of the ipsilateral tumor to 50 J/cm^2 of NIR light, 700 nm fluorescence signal of the tumor with irradiation of NIR light (NIR light (+)) was decreased in the dual NIR-PIT groups, while 700 nm fluorescence in the contralateral tumor (NIR light (–)) was unchanged (Supplementary Fig. S4C). Tumor growth was significantly suppressed in the dual NIR-PIT group compared with the I.V. group for not only NIR light (+) tumors but also NIR light (−) tumors ($p < 0.0001$ (both sides), vs I.V. group; Supplementary Fig. S4D). No significant difference was observed between the NIR light (+) and NIR light (−) tumor in each group. The survival of the dual NIR-PIT group was also significantly prolonged as compared to I.V. group (Supplementary Fig. S4E). Furthermore, complete remission of both side tumors using a one-sided dual-targeted NIR-PIT was achieved in 1 of 10 mice.

Discussion

In this study, we targeted CTLA4 expressing immuno-suppressive cells and hEGFR expressing cancer cells using anti-CTLA4 NIR-PIT and panitumumab-NIR-PIT, respectively. Simultaneous CTLA4/hEGFR dual-targeted NIR-PIT showed a stronger tumor response than either treatment alone even at the same antibody doses. The CD8$^+$/Treg ratio at 3 hours and 7 days after dual-targeted NIR-PIT was significantly increased compared with other therapies. Furthermore, abscopal effects were observed in a model of bilateral tumors after dual-targeted NIR-PIT. These results suggest that dual-targeted NIR-PIT can alter the immunosuppressive TME, resulted in strong synergistic effects on tumor growth suppression.

Although administration of unconjugated anti-hEGFR and anti-CTLA4 monotherapy has shown efficacy in various cancers, minimal therapeutic effects of the antibodies themselves was observed in this study (Fig. 3, 4, and S4). Indeed, since there was no change in the number of Tregs in the spleen (Fig. 2C and D), it is unlikely that anti-CTLA4 antibody

reduced the number of Tregs probably because less than half of the therapeutic antibody dose was used (7,27,34). However, a sizeable therapeutic effect was observed with dual-targeted NIR-PIT using the lower dose of anti-CTLA4 antibody. Serious autoimmune adverse effects associated with cancer immunotherapies including ICIs were frequently reported with anti-CTLA4 antibody (Ipilumumab) in humans (35–39). Ipilimumab is known to induce more frequent irAE than other ICIs particularly causing gastrointestinal symptoms in about 40% of patients when given at a dose of 3 mg/kg for melanoma therapy (24,40–43). The irAE of ipilimumab or pembrolizumab which blocks PD-L1, are reportedly dose-dependent (40,43,44). Therefore, low-dose administration of ICIs might minimize irAE. Thus, the dual-targeted NIR-PIT has a great advantage not only because of its superior therapeutic effects compared to ICIs but also because the antibody doses are predicted to have minimal adverse effects.

CTLA4 is expressed in FoxP3$^+$ Tregs and various other cells. Since the endocytosis of CTLA4 is extremely rapid (45–49), it is difficult to capture the expression of CTLA4 on the cell surface. Nevertheless, CTLA4-targeted NIR-PIT could still deplete Tregs within tumors. Furthermore, it has been reported that myeloid-derived suppressor cells and several kinds of cancer cells also expressed CTLA4 on the cell membrane (50–52). These cells could also be depleted by CTLA4-targeted NIR-PIT which could further enhance antitumor host immunity. Additionally, CTLA4-targeted NIR-PIT was reported to suppress intratumoral blood perfusion (26,53). Intra-tumoral blood flow reduction was observed after dual-targeted NIR-PIT similar to the monotherapy of CTLA4-targeted NIR-PIT (Supplementary Fig. S5). This early vascular effect might also contribute to the overall therapeutic effects.

CD25-targeted NIR-PIT also induced selective Treg depletion, however, because CD25 is the IL2 receptor, the presence of residual APC after the light exposure might block IL-2/IL-2R binding on activated effector cells resulting in their inhibition (25,34). CTLA4-targeted NIR-PIT might be superior to CD25-targeted NIR-PIT because anti-CTLA4 antibody did not block IL-2 binding and anti-CTLA4-IR700 would block the CTLA4 immune checkpoint pathway resulting in enhancement of host antitumor immunity (26). However, further research is needed to evaluate if the combination NIR-PIT with anti-CTLA4 actually is superior.

Dual-targeted NIR-PIT utilizing CTLA4 combined with CD44 as the cancer targeting agent was also evaluated, but no synergistic effects were observed in CD44 expressing LL/2-luc, MC38-luc, and MOC2-luc tumor models (Supplementary Fig. S2). There may be several reasons why the CTLA4/CD44 combination in these models was less effective than CTLA4/hEGFR in mEERL-hEGFR model. First, MC38-luc and LL/2-luc tumors are highly immunogenic tumors. Host tumor immunity was enhanced by CTLA4-targeted NIR-PIT alone possibly because the tumors were already highly infiltrated with lymphocytes before any treatment (Fig. 1E). In contrast, mEERL-hEGFR tumor was thought to be a poorly immunogenic tumor as indicated by the low-infiltration of T cells (Fig. 1E) and the lack of therapeutic effect of CTLA4-targeted NIR-PIT by itself. As expected, CTLA4/hEGFR dual-targeted NIR-PIT inhibited tumor progression in the mEERL-hEGFR allograft model and enhanced DC maturation and activation of T cell response (Fig. 4 and 5). Another reason would be off-target cell killing. MOC2-luc tumor was also poorly immunogenic

tumor, however, the synergistic effect of CTLA4/CD44 dual-targeted NIR-PIT was not seen in this model. It is known that CD44 is expressed not only on cancer cells but also on some immune cells, such as, effector T cells and memory T cells (47,54). We previously reported that CD44-positive subset of $CD8^+$ T cell was depleted by CD44-targeted NIR-PIT (18). Therefore, CD44-targeted NIR-PIT could also damage effector T cells, resulting in a weakened antitumor effect. On the other hand, NIR-PIT targeting hEGFR kills only hEGFR expressing cancer cells without damaging the host immune cells which do not express hEGFR (28). Thus, CTLA4/hEGFR dual-targeted NIR-PIT in the mEERL-hEGFR tumor model successfully induced anti-tumor immune activation by targeting only cancer cells and amplified the effect by eliminating CTLA4 expressing cells which are generally immune suppressive.

There are several limitations to this study. First, we used subcutaneously inoculated tumor models to evaluate the therapeutic effects of NIR-PIT. An orthotopic tumor models may be more clinically appropriate because they replicate the patients' TME more precisely. However, these models are technically difficult in evaluating the therapeutic effects in our experiments (55,56). Second, the dose of antibody or APC and the drug ratio (panitumumab: CTLA4=1:1) were fixed based on our previous experience. It is possible that other ratios of EGFR: CTLA4 targeting might be more or less efficacious. Additionally, we only investigated the therapeutic efficacy of simultaneously injected cocktails of APCs because we did not have to alter the procedures of injection and light exposure compared to controls. Since cancer cell-targeted NIR-PIT induces immunogenic cell death and CTLA4-targeted NIR-PIT activates tumor immunity by depleting immune suppressor cells, sequential, rather than simultaneous, cancer cell- and immune cell-targeted NIR-PIT at some appropriate interval might further improve the therapeutic outcome. We did not attempt this experiment because two sequential NIR-PIT procedures within a few days would be complicated and perhaps impractical for clinical translation. Nonetheless, CTLA4/hEGFR dual-targeted NIR-PIT successfully induced activation of host immunity resulting in tumor regression despite the fact that the mEERL-hEGFR tumor model is poorly immunogenic and typically shows less response to single-molecule-targeted therapy.

In conclusion, we show that CTLA4/hEGFR dual-targeted NIR-PIT successfully depleted cancer cells and CTLA4 expressing cells in the intratumoral tissues and had a significant impact on cell growth, surpassing that of either agent alone. This combined NIR-PIT approach has the potential to enhance therapeutic effects, especially when the efficacy of NIR-PIT monotherapy is unsatisfactory.

Supplementary Material

Refer to Web version on PubMed Central for supplementary material.

Acknowledgements:

This work was supported by the Intramural Research Program of the National Institutes of Health, National Cancer Institute, Center for Cancer Research [grant numbers ZIA BC 011513]

Abbreviation list:

NIR-PIT	near-infrared photoimmunotherapy
IR700	IRDye700DX
CTLA4	cytotoxic T-lymphocyte antigen 4
Tregs	regulatory T cells
mAb	monoclonal antibody
hEGFR	human epidermal growth factor receptor
APC	antibody-photoabsorber conjugate
ICD	immunogenic cell death
HER2	human epidermal growth factor receptor 2
PSMA	prostate-specific membrane antigen
CEA	carcinoembryonic antigen
ICI	immune checkpoint inhibitor
irAEs	immune-related adverse events

References

1. Mitsunaga M, Ogawa M, Kosaka N, Rosenblum LT, Choyke PL, Kobayashi H. Cancer cell-selective in vivo near infrared photoimmunotherapy targeting specific membrane molecules. Nat Med 2011;17:1685–91 [PubMed: 22057348]
2. Sato K, Ando K, Okuyama S, Moriguchi S, Ogura T, Totoki S, et al. Photoinduced Ligand Release from a Silicon Phthalocyanine Dye Conjugated with Monoclonal Antibodies: A Mechanism of Cancer Cell Cytotoxicity after Near-Infrared Photoimmunotherapy. ACS central science 2018;4:1559–69 [PubMed: 30555909]
3. Sato K, Watanabe R, Hanaoka H, Harada T, Nakajima T, Kim I, et al. Photoimmunotherapy: comparative effectiveness of two monoclonal antibodies targeting the epidermal growth factor receptor. Mol Oncol 2014;8:620–32 [PubMed: 24508062]
4. Sato K, Watanabe R, Hanaoka H, Nakajima T, Choyke PL, Kobayashi H. Comparative effectiveness of light emitting diodes (LEDs) and Lasers in near infrared photoimmunotherapy. Oncotarget 2016;7:14324–35 [PubMed: 26885688]
5. Ogata F, Nagaya T, Okuyama S, Maruoka Y, Choyke PL, Yamauchi T, et al. Dynamic changes in the cell membrane on three dimensional low coherent quantitative phase microscopy (3D LC-QPM) after treatment with the near infrared photoimmunotherapy. Oncotarget 2017;8:104295–302 [PubMed: 29262641]
6. Ogawa M, Tomita Y, Nakamura Y, Lee MJ, Lee S, Tomita S, et al. Immunogenic cancer cell death selectively induced by near infrared photoimmunotherapy initiates host tumor immunity. Oncotarget 2017;8:10425–36 [PubMed: 28060726]
7. Nagaya T, Friedman J, Maruoka Y, Ogata F, Okuyama S, Clavijo PE, et al. Host Immunity Following Near-Infrared Photoimmunotherapy Is Enhanced with PD-1 Checkpoint Blockade to Eradicate Established Antigenic Tumors. Cancer Immunol Res 2019;7:401–13 [PubMed: 30683733]

8. Kobayashi H, Choyke PL. Near-Infrared Photoimmunotherapy of Cancer. Acc Chem Res 2019;52:2332–9 [PubMed: 31335117]
9. Henderson TA, Morries LD. Near-infrared photonic energy penetration: can infrared phototherapy effectively reach the human brain? Neuropsychiatr Dis Treat 2015;11:2191–208 [PubMed: 26346298]
10. Wakiyama H, Kato T, Furusawa A, Choyke PL, Kobayashi H. Near infrared photoimmunotherapy of cancer; possible clinical applications. Nanophotonics-Berlin 2021
11. Kato T, Wakiyama H, Furusawa A, Choyke PL, Kobayashi H. Near Infrared Photoimmunotherapy; A Review of Targets for Cancer Therapy. Cancers (Basel) 2021;13 [PubMed: 35008178]
12. Nakajima K, Ogawa M. Phototoxicity in near-infrared photoimmunotherapy is influenced by the subcellular localization of antibody-IR700. Photodiagnosis and photodynamic therapy 2020;31:101926 [PubMed: 32717450]
13. Harada T, Nakamura Y, Sato K, Nagaya T, Okuyama S, Ogata F, et al. Near-infrared photoimmunotherapy with galactosyl serum albumin in a model of diffuse peritoneal disseminated ovarian cancer. Oncotarget 2016;7:79408–16 [PubMed: 27765903]
14. Sigismund S, Avanzato D, Lanzetti L. Emerging functions of the EGFR in cancer. Mol Oncol 2018;12:3–20 [PubMed: 29124875]
15. Oh DY, Bang YJ. HER2-targeted therapies - a role beyond breast cancer. Nature reviews Clinical oncology 2020;17:33–48
16. Nagaya T, Nakamura Y, Okuyama S, Ogata F, Maruoka Y, Choyke PL, et al. Syngeneic Mouse Models of Oral Cancer Are Effectively Targeted by Anti-CD44-Based NIR-PIT. Molecular cancer research: MCR 2017;15:1667–77 [PubMed: 28923838]
17. Wakiyama H, Furusawa A, Okada R, Inagaki F, Kato T, Maruoka Y, et al. Increased Immunogenicity of a Minimally Immunogenic Tumor after Cancer-Targeting Near Infrared Photoimmunotherapy. Cancers (Basel) 2020;12 [PubMed: 33375055]
18. Maruoka Y, Furusawa A, Okada R, Inagaki F, Fujimura D, Wakiyama H, et al. Near-Infrared Photoimmunotherapy Combined with CTLA4 Checkpoint Blockade in Syngeneic Mouse Cancer Models. Vaccines 2020;8
19. Nagaya T, Nakamura Y, Okuyama S, Ogata F, Maruoka Y, Choyke PL, et al. Near-Infrared Photoimmunotherapy Targeting Prostate Cancer with Prostate-Specific Membrane Antigen (PSMA) Antibody. Mol Cancer Res 2017;15:1153–62 [PubMed: 28588059]
20. Maawy AA, Hiroshima Y, Zhang Y, Heim R, Makings L, Garcia-Guzman M, et al. Near infra-red photoimmunotherapy with anti-CEA-IR700 results in extensive tumor lysis and a significant decrease in tumor burden in orthotopic mouse models of pancreatic cancer. PloS one 2015;10:e0121989 [PubMed: 25799218]
21. Shirasu N, Yamada H, Shibaguchi H, Kuroki M, Kuroki M. Potent and specific antitumor effect of CEA-targeted photoimmunotherapy. International journal of cancer 2014;135:2697–710 [PubMed: 24740257]
22. Hiroshima Y, Maawy A, Zhang Y, Guzman MG, Heim R, Makings L, et al. Photoimmunotherapy Inhibits Tumor Recurrence After Surgical Resection on a Pancreatic Cancer Patient-Derived Orthotopic Xenograft (PDOX) Nude Mouse Model. Ann Surg Oncol 2015;22 Suppl 3:S1469–74
23. Maawy AA, Hiroshima Y, Zhang Y, Garcia-Guzman M, Luiken GA, Kobayashi H, et al. Photoimmunotherapy lowers recurrence after pancreatic cancer surgery in orthotopic nude mouse models. J Surg Res 2015;197:5–11 [PubMed: 25799527]
24. Hodi FS, O'Day SJ, McDermott DF, Weber RW, Sosman JA, Haanen JB, et al. Improved survival with ipilimumab in patients with metastatic melanoma. The New England journal of medicine 2010;363:711–23 [PubMed: 20525992]
25. Sato K, Sato N, Xu B, Nakamura Y, Nagaya T, Choyke PL, et al. Spatially selective depletion of tumor-associated regulatory T cells with near-infrared photoimmunotherapy. Science translational medicine 2016;8:352ra110
26. Okada R, Kato T, Furusawa A, Inagaki F, Wakiyama H, Choyke PL, et al. Local Depletion of Immune Checkpoint Ligand CTLA4 Expressing Cells in Tumor Beds Enhances Antitumor Host Immunity. Advanced Therapeutics 2021;n/a:2000269

27. Maruoka Y, Furusawa A, Okada R, Inagaki F, Fujimura D, Wakiyama H, et al. Combined CD44- and CD25-Targeted Near-Infrared Photoimmunotherapy Selectively Kills Cancer and Regulatory T Cells in Syngeneic Mouse Cancer Models. Cancer Immunol Res 2020;8:345–55 [PubMed: 31953245]

28. Okada R, Furusawa A, Vermeer DW, Inagaki F, Wakiyama H, Kato T, et al. Near-infrared photoimmunotherapy targeting human-EGFR in a mouse tumor model simulating current and future clinical trials. EBioMedicine 2021;67:103345 [PubMed: 33933782]

29. Hoover AC, Spanos WC, Harris GF, Anderson ME, Klingelhutz AJ, Lee JH. The role of human papillomavirus 16 E6 in anchorage-independent and invasive growth of mouse tonsil epithelium. Arch Otolaryngol Head Neck Surg 2007;133:495–502 [PubMed: 17515506]

30. Spanos WC, Hoover A, Harris GF, Wu S, Strand GL, Anderson ME, et al. The PDZ binding motif of human papillomavirus type 16 E6 induces PTPN13 loss, which allows anchorage-independent growth and synergizes with ras for invasive growth. J Virol 2008;82:2493–500 [PubMed: 18160445]

31. Williams R, Lee DW, Elzey BD, Anderson ME, Hostager BS, Lee JH. Preclinical models of HPV+ and HPV- HNSCC in mice: an immune clearance of HPV+ HNSCC. Head Neck 2009;31:911–8 [PubMed: 19283850]

32. Mermod M, Hiou-Feige A, Bovay E, Roh V, Sponarova J, Bongiovanni M, et al. Mouse model of postsurgical primary tumor recurrence and regional lymph node metastasis progression in HPV-related head and neck cancer. International journal of cancer 2018;142:2518–28 [PubMed: 29313973]

33. Quezada SA, Peggs KS, Curran MA, Allison JP. CTLA4 blockade and GM-CSF combination immunotherapy alters the intratumor balance of effector and regulatory T cells. J Clin Invest 2006;116:1935–45 [PubMed: 16778987]

34. Okada R, Maruoka Y, Furusawa A, Inagaki F, Nagaya T, Fujimura D, et al. The Effect of Antibody Fragments on CD25 Targeted Regulatory T Cell Near-Infrared Photoimmunotherapy. Bioconjugate chemistry 2019;30:2624–33 [PubMed: 31498995]

35. Weber JS, D'Angelo SP, Minor D, Hodi FS, Gutzmer R, Neyns B, et al. Nivolumab versus chemotherapy in patients with advanced melanoma who progressed after anti-CTLA-4 treatment (CheckMate 037): a randomised, controlled, open-label, phase 3 trial. The Lancet Oncology 2015;16:375–84 [PubMed: 25795410]

36. Weber J, Mandala M, Del Vecchio M, Gogas HJ, Arance AM, Cowey CL, et al. Adjuvant Nivolumab versus Ipilimumab in Resected Stage III or IV Melanoma. The New England journal of medicine 2017;377:1824–35 [PubMed: 28891423]

37. Robert C, Thomas L, Bondarenko I, O'Day S, Weber J, Garbe C, et al. Ipilimumab plus dacarbazine for previously untreated metastatic melanoma. The New England journal of medicine 2011;364:2517–26 [PubMed: 21639810]

38. Quirk SK, Shure AK, Agrawal DK. Immune-mediated adverse events of anticytotoxic T lymphocyte-associated antigen 4 antibody therapy in metastatic melanoma. Translational research : the journal of laboratory and clinical medicine 2015;166:412–24 [PubMed: 26118951]

39. Hodi FS, O'Day SJ, McDermott DF, Weber RW, Sosman JA, Haanen JB, et al. Improved survival with ipilimumab in patients with metastatic melanoma. The New England journal of medicine 2010;363:711–23 [PubMed: 20525992]

40. Dougan M, Blidner AG, Choi J, Cooksley T, Glezerman I, Ginex P, et al. Multinational Association of Supportive Care in Cancer (MASCC) 2020 clinical practice recommendations for the management of severe gastrointestinal and hepatic toxicities from checkpoint inhibitors. Support Care Cancer 2020;28:6129–43 [PubMed: 32856210]

41. Dougan M.Checkpoint Blockade Toxicity and Immune Homeostasis in the Gastrointestinal Tract. Frontiers in immunology 2017;8:1547 [PubMed: 29230210]

42. Eggermont AM, Chiarion-Sileni V, Grob JJ, Dummer R, Wolchok JD, Schmidt H, et al. Prolonged Survival in Stage III Melanoma with Ipilimumab Adjuvant Therapy. The New England journal of medicine 2016;375:1845–55 [PubMed: 27717298]

43. Puzanov I, Diab A, Abdallah K, Bingham CO 3rd, Brogdon C, Dadu R, et al. Managing toxicities associated with immune checkpoint inhibitors: consensus recommendations from the Society for

Immunotherapy of Cancer (SITC) Toxicity Management Working Group. J Immunother Cancer 2017;5:95 [PubMed: 29162153]

44. Maughan BL, Bailey E, Gill DM, Agarwal N. Incidence of Immune-Related Adverse Events with Program Death Receptor-1- and Program Death Receptor-1 Ligand-Directed Therapies in Genitourinary Cancers. Front Oncol 2017;7:56 [PubMed: 28421161]
45. Chen DS, Mellman I. Elements of cancer immunity and the cancer-immune set point. Nature 2017;541:321–30 [PubMed: 28102259]
46. Verma N, Burns SO, Walker LSK, Sansom DM. Immune deficiency and autoimmunity in patients with CTLA-4 (CD152) mutations. Clinical and experimental immunology 2017;190:1–7 [PubMed: 28600865]
47. Topham DJ, Reilly EC. Tissue-Resident Memory CD8(+) T Cells: From Phenotype to Function. Frontiers in immunology 2018;9:515 [PubMed: 29632527]
48. Rowshanravan B, Halliday N, Sansom DM. CTLA-4: a moving target in immunotherapy. Blood 2018;131:58–67 [PubMed: 29118008]
49. Qureshi OS, Kaur S, Hou TZ, Jeffery LE, Poulter NS, Briggs Z, et al. Constitutive clathrin-mediated endocytosis of CTLA-4 persists during T cell activation. The Journal of biological chemistry 2012;287:9429–40 [PubMed: 22262842]
50. Yu GT, Bu LL, Zhao YY, Mao L, Deng WW, Wu TF, et al. CTLA4 blockade reduces immature myeloid cells in head and neck squamous cell carcinoma. Oncoimmunology 2016;5:e1151594 [PubMed: 27471622]
51. Pico de Coana Y, Masucci G, Hansson J, Kiessling R. Myeloid-derived suppressor cells and their role in CTLA-4 blockade therapy. Cancer immunology, immunotherapy : CII 2014;63:977–83 [PubMed: 24966003]
52. Chaudhary B, Elkord E. Regulatory T Cells in the Tumor Microenvironment and Cancer Progression: Role and Therapeutic Targeting. Vaccines 2016;4
53. Kurebayashi Y, Olkowski CP, Lane KC, Vasalatiy OV, Xu BC, Okada R, et al. Rapid Depletion of Intratumoral Regulatory T cells Induces Synchronized CD8 T and NK Cell Activation and IFN-γ-dependent Tumor Vessel Regression. Cancer research 2021
54. Govindaraju P, Todd L, Shetye S, Monslow J, Pure E. CD44-dependent inflammation, fibrogenesis, and collagenolysis regulates extracellular matrix remodeling and tensile strength during cutaneous wound healing. Matrix biology : journal of the International Society for Matrix Biology 2019;75–76:314–30
55. Hoffman RM. Patient-derived orthotopic xenografts: better mimic of metastasis than subcutaneous xenografts. Nat Rev Cancer 2015;15:451–2 [PubMed: 26422835]
56. Hoffman RM. Orthotopic metastatic mouse models for anticancer drug discovery and evaluation: a bridge to the clinic. Invest New Drugs 1999;17:343–59 [PubMed: 10759402]

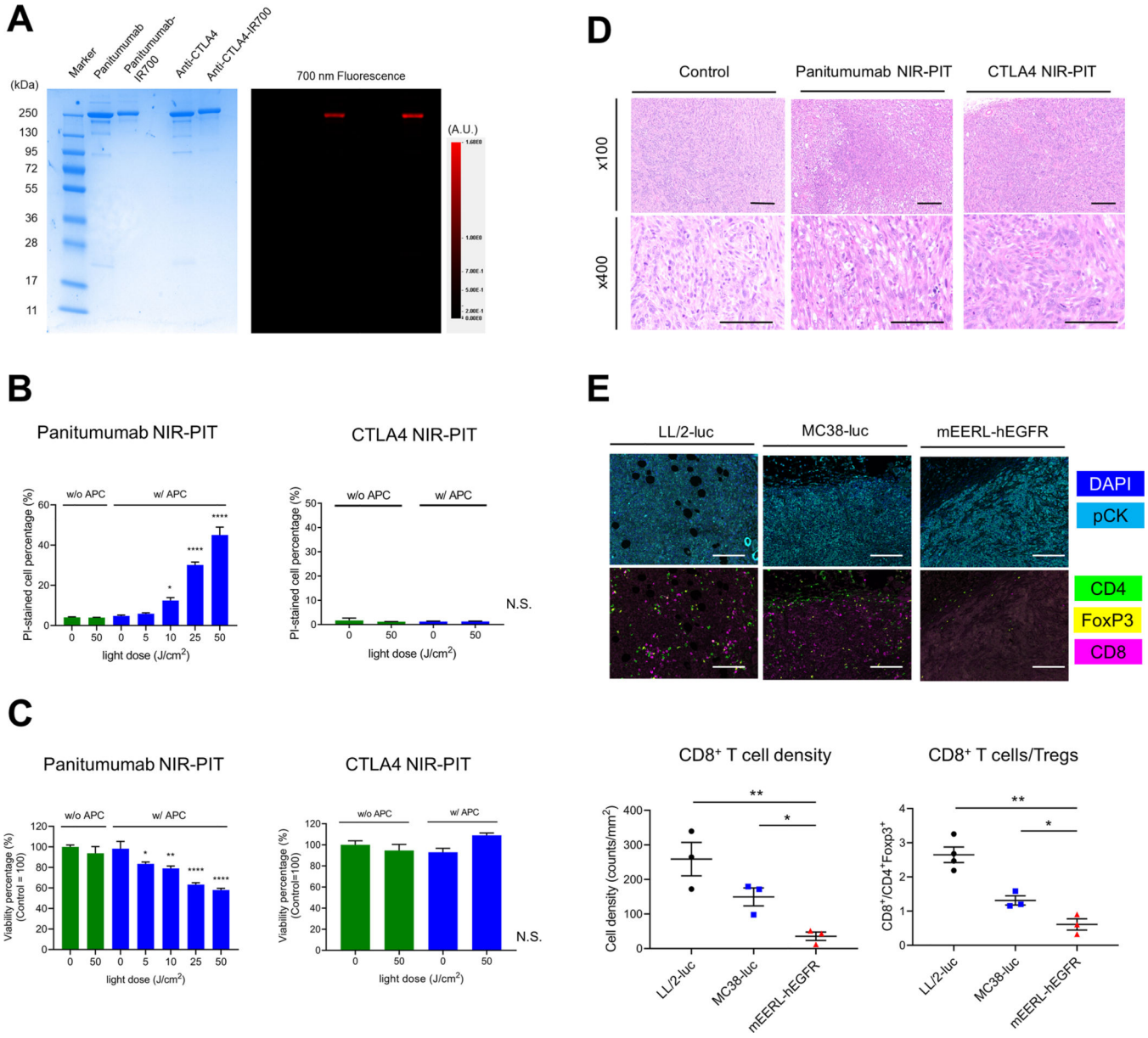

Figure 1.

Characteristics of the mEERL-hEGFR cell line and evaluation by panitumumab- or CTLA4-targeted NIR-PIT

A, Validation of panitumumab-IR700 and CTLA4-IR700 by SDS-PAGE (left: Colloidal Blue staining, right: 700 nm fluorescence). Each diluted antibody was used as a control.

B, Membrane damage of mEERL-hEGFR cells induced by NIR-PIT was measured using PI staining. Each value represents means ± SEM of independent experiments.

C, Metabolic activity measured by MTT assay. Control groups either had no APC administration or NIR light irradiation only. Each value represents the mean (% of control mean) ± SEM of independent experiments. **D,** Histological evaluation with H-E staining. Panitumumab NIR-PIT induced swelling and vacuolation of the tumor cells within one hour after light exposure, while CTLA4 NIR-PIT induced no obvious changes. Scale bars

represent 100 μm (upper images) or 50 μm (lower images). **E,** Representative multiplex immunohistochemistry images of LL/2-luc, MC38-luc, and mEERL-hEGFR tumors. Upper panels show composite images of pCK and DAPI staining, lower panels show composite images of CD4, FoxP3, and CD8 staining. Intratumoral $CD8^+$ T cells were counted in multiplex IHC images. Data are shown as cell count per mm^2. Intratumoral $CD8^+$ T cell density was significantly lower in mEERL-hEGFR tumors than in the other tumors. Intratumoral $CD8^+$/Treg ratio was also lower in mEERL-hEGFR tumors compared with the other tumors (Images; ×200, scale bar = 100 μm. n = 4; one-way ANOVA followed by Tukey's test; *, $p < 0.05$; **, $p < 0.01$; N.S., not significant).

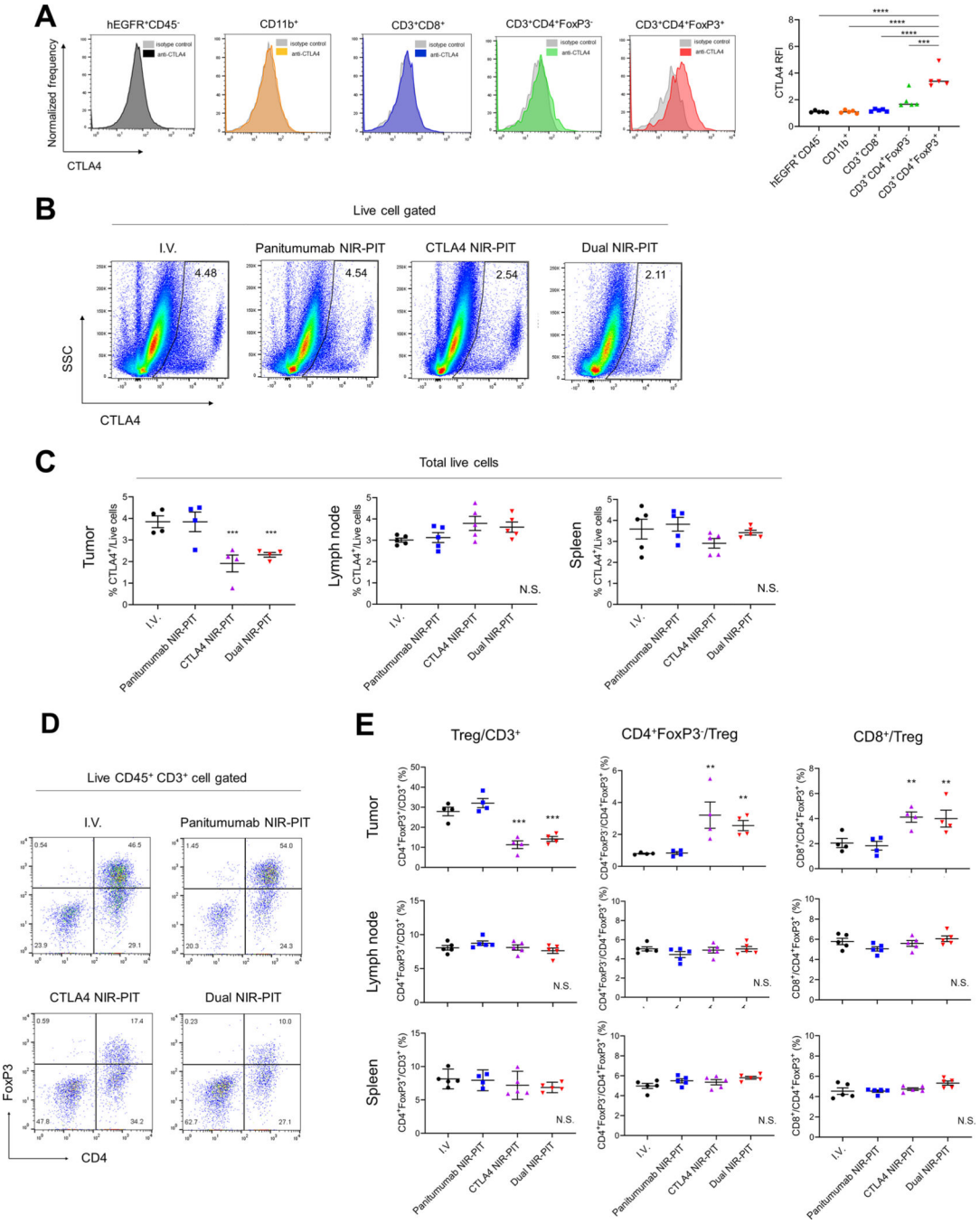

Figure 2.

Depletion of CTLA4 expressing cells by dual-targeted NIR-PIT.

A, CTLA4 expression of several cells in mEERL-hEGFR tumors was analyzed by flow cytometry. Representative histograms for CTLA4 expression in tumor cells ($hEGFR^+CD45^-$), $CD11b^+$ cells, $CD8^+$ T cells ($CD3^+CD8^+$), $CD4^+FoxP3^-$ T cells, and Tregs ($CD3^+CD4^+FoxP3^+$) and RFI of CTLA4 are shown (n = 5; one-way ANOVA followed by Tukey's test; *, $P < 0.05$; **, $P < 0.01$; ****, $P < 0.0001$). **B,** Representative dot plots show CTLA4 expression in live cells within mEERL-hEGFR tumors with flow

cytometry three hours after each NIR-PIT. **C,** The percentages of $CTLA4^+$ cells among total live cells within mEERL-hEGFR tumors, tumor draining lymph nodes, and spleens. CTLA4 expressing cells within tumor after CTLA4 NIR-PIT or dual NIR-PIT were significantly decreased. **D,** Representative dot plots show Treg populations within mEERL-hEGFR tumors 3 hours after each NIR-PIT. **E,** Scatter plots show the Treg/$CD3^+$, non-regulatory $CD4^+$ ($CD4^+FoxP3^-$)/Treg, and $CD8^+$/Treg ratios within tumors, tumor draining lymph nodes, and spleens. In CTLA4 and dual NIR-PIT groups, the Treg/$CD3^+$ ratio is significantly decreased, whereas the $CD4^+$/Treg and $CD8^+$/Treg ratios are increased. (n = 4; one-way ANOVA followed by Tukey's test; **, $P < 0.01$; ***, $P < 0.001$; N.S., not significant).

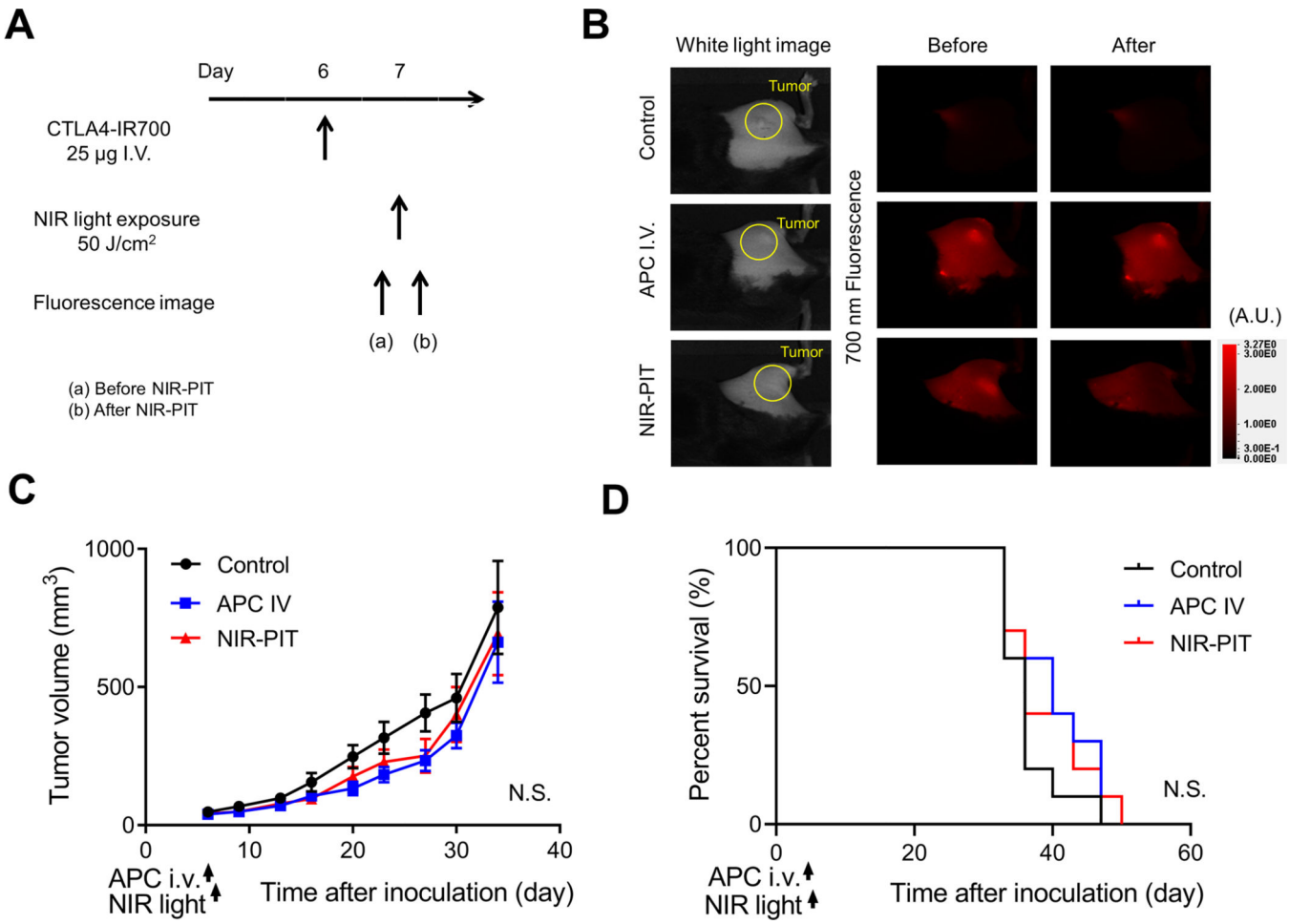

Figure 3.

Efficacy of *in vivo* CTLA4-targeted NIR-PIT of mEERL-hEGFR tumors.

A, Treatment schedule. **B,** 700 nm fluorescent imaging before and after NIR-PIT in mEERL-hEGFR tumor-bearing mouse (A.U., arbitrary units). **C,** Tumor volume curves (n = 10; mean ± SEM; repeated measures two-way ANOVA followed by Tukey's test; N.S., not significant). **D,** Survival curves (n = 10; log-rank test with Bonferroni correction; N.S., not significant).

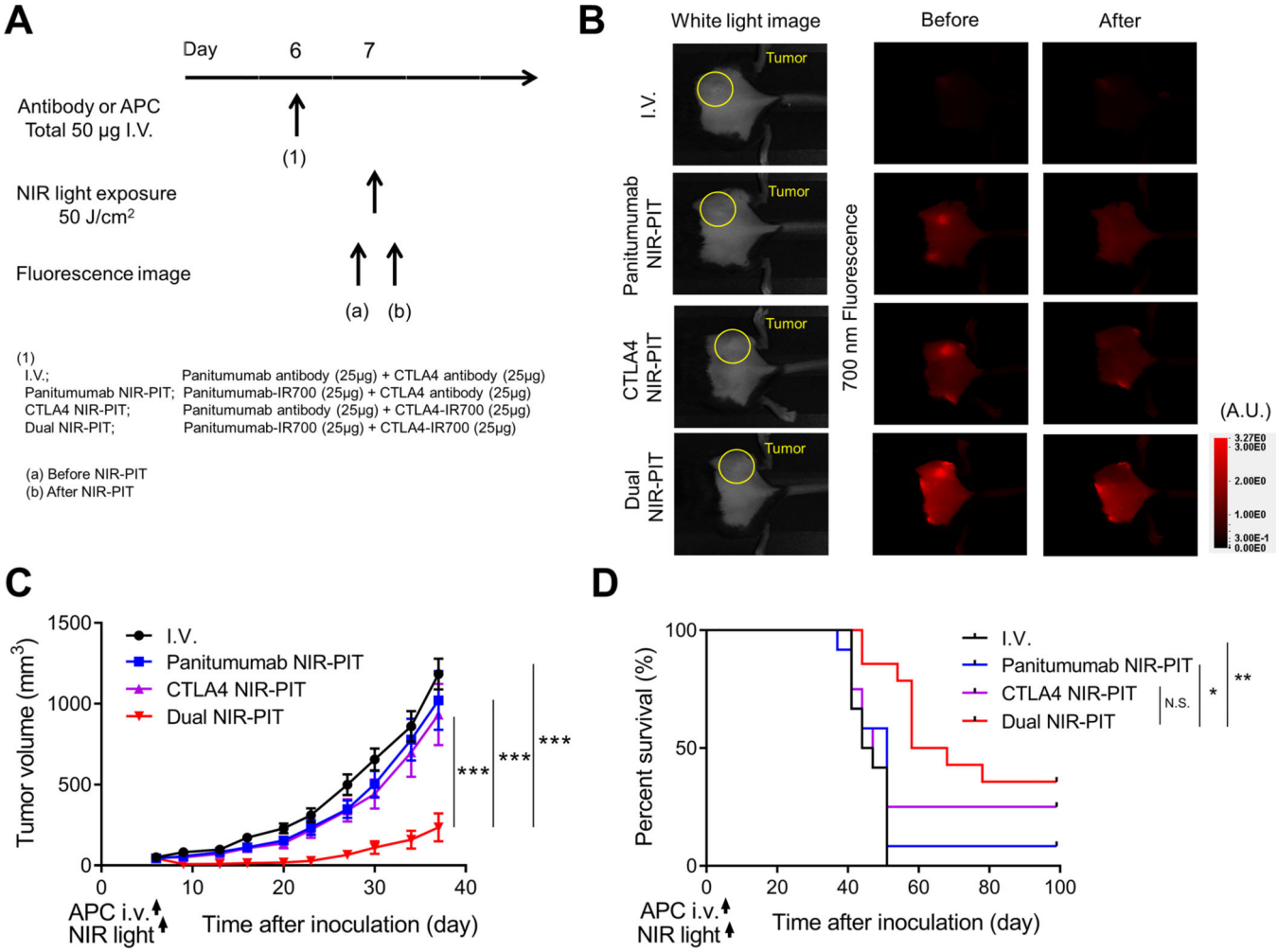

Figure 4.

Efficacy of *in vivo* combined NIR-PIT targeting hEGFR and CTLA4.

A, Treatment schedule. **B,** 700 nm fluorescent imaging before and after NIR-PIT in mEERL-hEGFR tumor-bearing mouse (A.U., arbitrary units). The 700 nm fluorescence of the tumor decreased immediately after light exposure except for the I.V. group. Yellow circles represent the locations of tumors. **C,** Tumor volume curves (n =12–13; mean ± SEM; repeated measures two- way repeated measures ANOVA followed by Tukey's test, *, $p < 0.05$; **, $p < 0.01$; ***, $p < 0.001$, vs. dual NIR-PIT group). **D,** Survival curves (n = 12–13, log-rank test with Bonferroni correction; *, $p < 0.05$; **, $p < 0.01$; N.S., not significant). The panitumumab NIR-PIT, CTLA4 NIR-PIT, and dual NIR-PIT cleared the tumor in 1/12, 3/12, 5/13 mice, respectively.

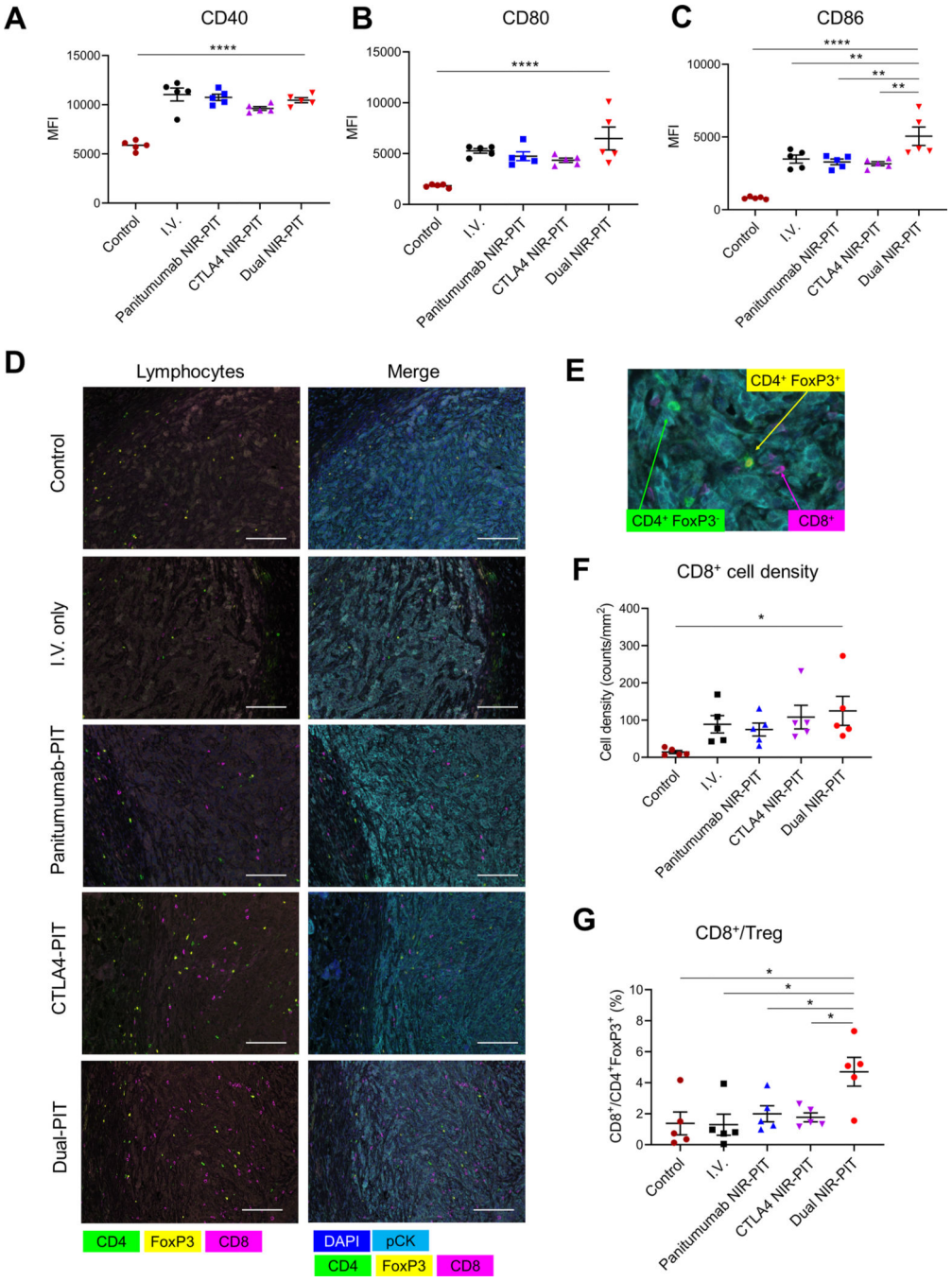

Figure 5.

Dual-targeted NIR-PIT improved the immunosuppressive environment within mEERL-hEGFR tumors.

A-C, Cell populations in the regional lymph nodes were analyzed 2 days after each NIR-PIT by flow cytometry in the mEERL-hEGFR model. The expression of activation markers (CD40 (**A**), CD80 (**B**), CD86(**C**)) on dendritic cells was assessed. CD86 expression in the dual NIR-PIT group is significantly higher compared with any other group. **D,** Multiplex immunohistochemical staining of the tumors 7 days after NIR light exposure.

Right: lymphocyte marker staining; CD8 (magenta), CD4 (green) and FoxP3 (yellow). Left: Merged images. Scale bar, 100 μm. **E,** Examples of $CD8^+$ T cell (magenta arrow), $CD4^+FoxP3^-$ T cell (green arrow) and Treg ($CD4^+FoxP3^+$ cell) (yellow arrow). **F,** Intratumoral $CD8^+$ T cell density was significantly higher in the dual NIR-PIT group than the control group (n = 5, one-way ANOVA followed with Tukey's test; *, $p < 0.05$). **G,** Intratumoral $CD8^+$/Treg ratio was also increased in the dual NIR-PIT group compared with any other group (n = 5, one-way ANOVA followed with Tukey's test; *, $p < 0.05$; vs. dual NIR-PIT group).

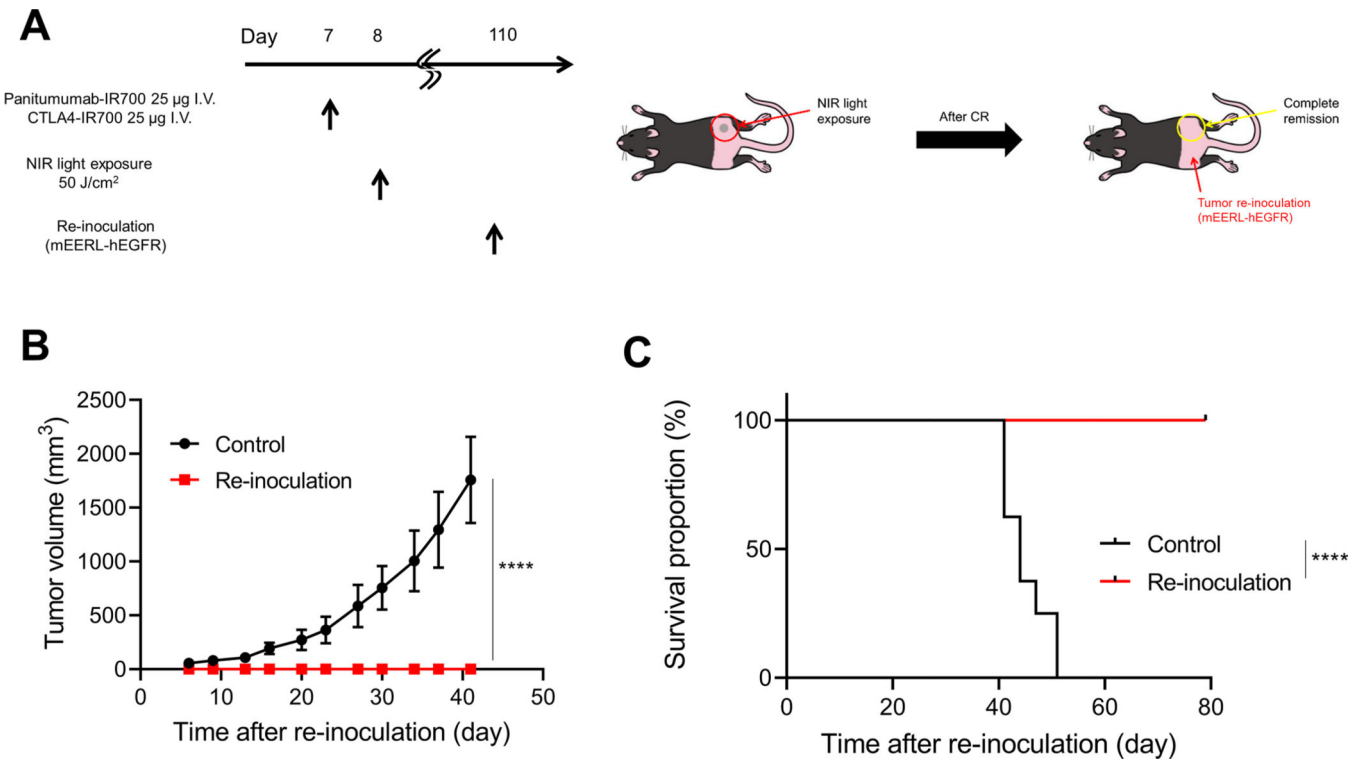

Figure 6.

Dual-targeted NIR-PIT induced long-term immunity against mEERL-hEGFR tumor. The mice that achieved complete remission by dual-targeted NIR-PIT were re-inoculated with mEERL-hEGFR tumor in the contralateral flank. **A,** Treatment schedule and location of re-inoculation. **B,** Tumor volume curves. Control = newly inoculated tumor; Re-inoculation = re-inoculated tumor after complete clearance by dual NIR-PIT (n =5; mean ± SEM; repeated measures two-way repeated measures ANOVA followed by Tukey's test; ****, $p < 0.0001$). **C,** Survival curves (log-rank test; ****, $p < 0.0001$).